# Self-consistent kinetic simulation of plasmas

J. Feng and W. N. G. Hitchon
*Electrical and Computer Engineering, University of Wisconsin at Madison, Madison, Wisconsin 53706-1691*
(Received 11 October 1999)

An improved version of a kinetic simulation technique, the convected scheme (CS), is described. We present a ''long-lived moving cell'' version of the convected scheme and describe a recipe for implementation in detail. In collisional systems, the numerical diffusion in ''ballistic motion'' does not affect the simulation result of the regular CS, which can be set up to minimize numerical diffusion in collision processes. With the new scheme, the numerical diffusion is highly reduced even in nearly collisionless plasma systems, which is important in the modeling of low-pressure high-density plasma sources.

PACS number(s): 02.70.−c, 52.65.−y, 52.25.Dg

## I. INTRODUCTION

Kinetic models are essential for accurate description of the energy and velocity distributions of the particle species in a plasma. There are several kinetic models, each having its own advantages and limitations. Several particle type methods, such as Monte Carlo, direct simulation Monte Carlo, and particle in cell [1] are well developed. The other main type of model involves solving the plasma kinetic equation. The convected scheme (CS) model has been used in simulations of both fusion [2] and processing [3,4] plasmas. It is a formidable task to obtain a solution of a realistic discharge due to the difficulty of describing the charged-particle behavior consistently with the fields present, the wide range of time scales present, and limited basic cross-section and reaction rate data. Regardless of these obstacles, it was found that the major source of error in the CS is numerical diffusion.

The purpose of this paper is, in part, to investigate the accuracy of a class of schemes for kinetic simulation of plasmas. The class we consider here are direct solutions of the Boltzmann equation. We thus do not consider simulations of the ''particle'' type [5]. Such particle simulations allow very accurate tracking of individual particles, but suffer from statistical noise and from poor sampling of some regions of both physical and velocity space. In the past some of the major sources of error in the most accurate type of scheme for solving the Boltzmann equation have been considered [6]—which are probably schemes based on the method of characteristics. The errors associated with the ''ballistic'' motion (i.e., the motion in phase space in the absence of collisions) were discussed, as well as the errors involved in the handling of collisions, and it was argued that different sets of phase-space variables were optimal for the handling of each of these two processes.

It was pointed out that conservation of particles and energy are usually critical for an accurate simulation, and for these to be implemented, locally in phase space, we need to track particles leaving an 'initial' cell on the mesh and impose the conservation law(s) whenever those particles are put back onto the mesh. Nonconservation of particles is clearly a severe problem—especially in a simulation where the Poisson equation is solved, since if particle numbers grow artificially, the electric field will almost certainly be greatly in error. However, a small but steady artificial input of energy can also lead to nonsensical results, since the ionization rate may then grow without bounds. It was pointed out that the lowest energy particles are the most troublesome to simulate. This is perhaps not surprising at one level, since their very slow motion makes the simulation of these particles the most numerically ''stiff'' aspect of the scheme. In addition, the need to use an energy conserving scheme causes special problems for particles that do not leave the initial spatial cell, before they are mapped back. If we do not conserve energy when we update their coordinates, then particles that are put back in a given cell [i.e., with spatial coordinate(s) unchanged] can have gained energy. Over many repetitions of this mapping back, they can gain a lot of energy, quite artificially. On the other hand, if we do conserve their energy, then if they are put back in the same spatial cell, they are effectively put back at the cell center (since we cannot distinguish their location better than this, once they are back in the cell) and so they lose any energy they gained in the last step. This means that they stay in the cell too long, since their acceleration is repeatedly negated at the end of each time step. Because of this dilemma, in particular, and because numerical diffusion is a problem whenever the phase fluid is mapped back, we investigate the use of ''long lived moving cells'' (LLMC). These are simply packets of phase fluid that persist for more than one time step, and they usually last until the packet gets out of its initial spatial cell or until a collision time has elapsed (so the packet is largely emptied out by collisions, as we shall see). We introduce this new scheme in kinetic modeling for low-pressure partially ionized plasmas, and summarize it in a detailed recipe. This algorithm is first benchmarked by imposing a constant field (swarm) configuration and comparing with experiments. A set of rf helium discharge simulations will also be used as benchmarks.

## II. KINETIC MODELS

Kinetic models can be divided into two categories: statistical models and direct solutions of the Boltzmann transport equation [7]. Monte Carlo, DSMC, and PIC are of the former type. They use random number generators to simulate the effects of collisions; and integrate the equations of motion to track particle movements. Sometimes statistical noise will reduce the quality of the simulation results.

 

The other type of kinetic modeling requires us to find the solution of a kinetic equation directly. One approach is using a Fourier transform of the kinetic equation, then solving the dynamic equations for the Fourier coefficients [8–10]. Another approach is to solve the kinetic equations directly, as is done in the convected scheme (CS) method.

The CS uses the method of characteristics to construct propagators [11–14]. After a brief introduction to the methodology of the CS, we will describe the details of the improvements we have made to the CS and give the recipe for its implementation.

### A. Propagator method

The kinetic behavior of a gas discharge is described by the *Boltzmann (transport) equation*:

$$\frac{\partial f}{\partial t}+\boldsymbol{v}\cdot\frac{\partial f}{\partial \boldsymbol{x}}+\boldsymbol{a}\cdot\frac{\partial f}{\partial \boldsymbol{v}}=C(f), \tag{1}$$

where, for each species, $f=f(\boldsymbol{x},\boldsymbol{v},t)$ is the one-particle distribution function, which statistically describes the number of particles in the volume $d\boldsymbol{x}\,d\boldsymbol{v}$ at the position $(\boldsymbol{x},\boldsymbol{v})$ in the six-dimensional phase space at time t, $\boldsymbol{a}$ is the *ensemble*-averaged acceleration, and $C(f)$ is the collision operator. The CS is based on using the propagator method to solve the Boltzmann equation for the (one-particle) distribution function.

For each particle species the formal solution of the Boltzmann equation for short time steps can be written as:

$$f(\boldsymbol{x},\boldsymbol{v},t)=\int\int \mathcal{P}(\boldsymbol{x},\boldsymbol{v},t;\boldsymbol{x}',\boldsymbol{v}',t')f(\boldsymbol{x}',\boldsymbol{v}',t')d\boldsymbol{x}'d\boldsymbol{v}', \qquad t>t', \tag{2}$$

where the kernel of the integral, $\mathcal{P}(\boldsymbol{x},\boldsymbol{v},t;\boldsymbol{x}',\boldsymbol{v}',t')$, is the propagator for a particle at the phase space position $(\boldsymbol{x}',\boldsymbol{v}')$ at time $t'$ moving to $(\boldsymbol{x},\boldsymbol{v})$ at a later time $t$. Certain properties and conservation laws related to this propagator in the CS were noted by Adams *et al.* [11]. Instead of finding the explicit form of the propagator in a 14-dimensional space, the CS propagator is divided into two parts—one for the ballistic motion and one for collisions. In the ballistic motion collisions are neglected, and the Boltzmann equation is reduced to the *Vlasov equation*:

$$\frac{df}{dt}=\frac{\partial f}{\partial t}+\boldsymbol{v}\cdot\frac{\partial f}{\partial \boldsymbol{x}}+\boldsymbol{a}\cdot\frac{\partial f}{\partial \boldsymbol{v}}=0. \tag{3}$$

In the CS, the Vlasov equation is numerically integrated along the *characteristic curves*, which are determined by the equations of motion: $d\boldsymbol{x}/dt=\boldsymbol{v}$ and $d\boldsymbol{v}/dt=\boldsymbol{a}$. After this ballistic motion step is complete for all particle species, $f$ is adjusted according to the collision processes described by the collision operators $C(f)$ as well as chemical reactions.

While particle methods, such as Monte Carlo and particle-in-cell models, use super particles, the CS uses cells. The superparticles are (usually) unbreakable entities and collide statistically by using random number generators. Statistical noise in the number of particles in a small region of phase-space can be a significant issue in such particle methods. On the contrary, the CS is free of statistical noise, but the finite size and the discreteness of the phase space mesh will cause *numerical diffusion*, when particles from cells are redistributed after the ballistic motion or after collisions. The *long-lived moving cell* (LLMC) model has been conceived to reduce the numerical diffusion, by reducing the number of times this redistribution occurs.

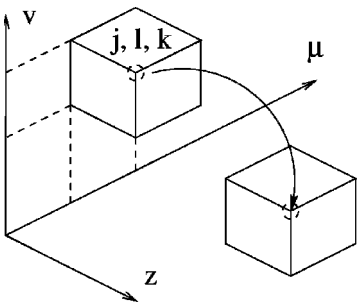


FIG. 1. Mesh for three-dimensional phase space.

### B. Convected scheme using long-lived moving cells

The idea of the CS is, given a suitable numerical mesh throughout phase space, to move the particles associated with the individual cells of the mesh to a new location based on their coordinates (position and velocity), the fields present, the collision probability, and the time step. We shall give a three-dimensional example (1D-space and 2D-velocity) for the electron ballistic-mover. Conservation laws that significantly affect simulation results will be emphasized. After describing the design of the mesh, we will introduce the CS with LLMC's, as well as how numerical diffusion can be reduced by this new scheme. Other possibilities to improve the current version of the CS with LLMC's will be discussed later. Finally, we will summarize the ion ballistic mover, which is similar but simpler.

It is assumed that the distance between two plane parallel electrodes is much less than the lateral dimensions of the electrodes so that fringing effects can be ignored. We use $(z,v,\mu)$ to construct the three-dimensional phase-space mesh (Fig. 1). The position along the spatial $z$ axis, which is perpendicular to the plates, is denoted by $z$. The speed of electrons is denoted by $v$, and the direction cosine of the velocity relative to the $z$ axis by $\mu$. The finite-ranged phase space is divided into cells. Each cell, labeled by indices $(j,l,k)$ on the phase-space mesh, is associated with a single set of $(z|_j,v|_l,\mu|_k)$. We will use the terms ''mesh cell'' to describe a cell fixed on the mesh, ''initial cell'' a cell before the ballistic motion carries it away from its mesh cell, ''moving cell'' the same cell during or after the ballistic motion, and ''final cells'' those mesh cells overlapped by a moving cell at the end of its ballistic motion. The particles in the mesh cell $(j,l,k)$ have unique $v|_l$ and $\mu|_k$ values, and are distributed uniformly in the spatial range $\Delta z|_j$ with average value $z|_j$. Similarly, the particles in each moving cell are assumed distributed uniformly in space but with constant $v$ and $\mu$ instead of over a range of $v$ and $\mu$ values. Figure 2 is a schematic of the movement of the phase-space cells during a time step.

The initial cell centered at $(z'',v'',\mu'')$ is moved according to the equations of motion:

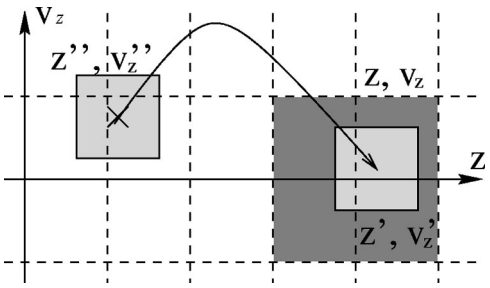


FIG. 2. Schematic of ''ballistic'' propagator in three dimensions.

$$\frac{d\boldsymbol{x}}{dt}=\boldsymbol{v} \tag{4}$$

$$\frac{d\boldsymbol{v}}{dt}=\frac{q}{m}(\boldsymbol{E}+\boldsymbol{v}\times\boldsymbol{B}) \tag{5}$$

to a new position $(z',v',\mu')$ in the phase space, where it overlaps with neighboring final cells at $(z,v,\mu)$. The Euler scheme is employed to integrate these two equations of the motion, i.e., $\boldsymbol{E}$ and $\boldsymbol{B}$ are evaluated at the initial cell center $z''$ in Eq. (4) and Eq. (5), except that the final $z$ component of the velocity $v_z'$ is computed by energy conservation. Specifically, for this one-dimensional system, we know that the ''$z$ component'' of the total energy is conserved in the ballistic motion, so

$$\frac{1}{2}mv_z'^2=\frac{1}{2}mv_z''^2+q\Phi(z'')-q\Phi(z'), \tag{6}$$

where $\Phi(z'')$ and $\Phi(z')$ are based on the initial potential profile and $v_z'=v'\mu', v_z''=v''\mu''$.

In this numerical enforcement of the conservation of energy, the initial potential profile was interpreted as a staircase potential in the regular CS (that is, the potential is considered constant in each spatial cell). However, using the CS with LLMC's can affect the convergence of some simulation results, especially when the parameters of the discharge are on the boundary of the working range—that is, when the real discharge is only marginally able to sustain itself. To model particle dynamics more precisely, a curve-fitted potential (CFP) is sometimes used when calculating the energy at the location of the centers of LLMC's. If the CFP at the final cell center, $\Phi(z')$, implies that the location $z'$ is energetically forbidden, the electrons retrace their trajectory by using a smaller time step. This reduction of time step has to be terminated after several orders if the desired accuracy is not achieved. Other time integration methods, such as the leap-frog scheme or the Runge-Kutta scheme [5], can replace the Euler scheme. Although the leap-frog scheme has a wider range of numerical stability for different simulation parameters or time steps, the simulation results from it are essentially the same as those from the Euler scheme. The numerical enforcement of the conservation of energy has a more profound effect on the simulations than the integration scheme does.

Due to the limitation of computer memory the regular CS requires periodic remapping of the particles in a moving cell onto the mesh cells, which have discrete coordinates in the phase space. Typically, moving cells do not correspond exactly to mesh cells; particles with a unique position in the phase space have to be shared among neighboring mesh cells, and this gives rise to the artificial numerical diffusion. To reduce the numerical diffusion during the ballistic move, a train of LLMC's is launched, one cell usually being the most launched at each time step for each mesh cell. Other techniques, which launch LLMC's less often, are also investigated and will be described in more detail later. (See Fig. 3.) Since the number of (unscattered) particles in a moving cell decays exponentially with time, the number of particles that remain in the last moving cell depends on the length of the train. Particles in the leading moving cell of each train will be remapped back to the mesh cells when a new moving cell is added to the train. For particles in these LLMC's, which are as yet unscattered, the remapping happens less frequently compared to the regular CS, so numerical diffusion due to ballistic motion will be highly reduced. Ideally, the leading moving cell of the train will have existed for about 1 to 2 collision times, so 60–90 % of the particles that were in it initially will have scattered out before it is remapped. The errors involved in remapping those particles that have collided make it pointless to follow the unscattered particles for much more than one collision time.

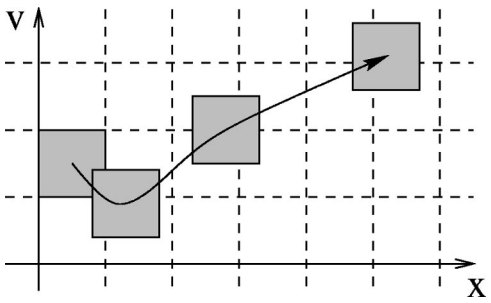


FIG. 3. Launching a new moving cell.

As shown in Fig. 4, electrons in the moving cell at $(z',v',\mu')$ are shared between the neighboring cells on the $(z,v)$ mesh, cells *A*, *B*, *C*, and *D*. Particle number and kinetic energy are conserved, if the fractions of particles for each final cell are:

$$F_A=\left(\frac{z|_{i+1}-z'}{z|_{i+1}-z|_i}\right)\left(\frac{(v_i')^2-v|_j^2}{v|_{j+1}^2-v|_j^2}\right) \tag{7}$$

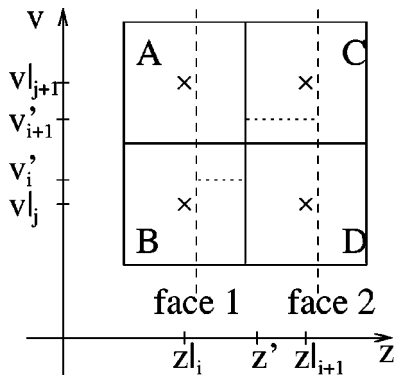


FIG. 4. Redistributing particles in a moving cell back to the mesh cells *A*, *B*, *C*, and *D*.

$$F_B=\left(\frac{z|_{i+1}-z'}{z|_{i+1}-z|_i}\right)\left(\frac{v|_{j+1}^2-(v_i')^2}{v|_{j+1}^2-v|_j^2}\right) \tag{8}$$

$$F_C=\left(\frac{z'-z|_i}{z|_{i+1}-z|_i}\right)\left(\frac{(v_{i+1}')^2-v|_j^2}{v|_{j+1}^2-v|_j^2}\right) \tag{9}$$

$$F_D=\left(\frac{z'-z|_i}{z|_{i+1}-z|_i}\right)\left(\frac{v|_{j+1}^2-(v_{i+1}')^2}{v|_{j+1}^2-v|_j^2}\right), \tag{10}$$

where $(v_i')^2=(v')^2+(2q/m)\Phi(z')-(2q/m)\Phi(z|_i)$ and $(v_{i+1}')^2=(v')^2+(2q/m)\Phi(z')-(2q/m)\Phi(z|_{i+1})$. (Note the order of remapping: we spread the particles over space, then we conserved kinetic energy in each spatial cell.) For each spatial cell, particles are in addition distributed over $v$ and $\mu$ cells such that the ''parallel component'' and ''perpendicular component'' of the averaged kinetic energy are unchanged. If one of the spatial cells is energetically forbidden, $\frac{1}{2}m(\mu' v')^2+q\Phi(z')<q\Phi(z|_i)$ or $q\Phi(z|_{i+1})$, the particles are remapped to the other spatial cell, with newly calculated $v$ and $v_z$. In the case of reflection, the sign of $v_z$ is reversed.

After the ballistic motion step, to calculate the rates of collision processes and chemical reactions, the velocities of electrons for each moving cell are determined in the overlapped final cells. For the regular CS, the kinetic energy corresponding to the velocity determines collision rates or chemical reaction rates in a final cell, using the staircase potential. In Fig. 4, the percentage of scattered particles for the part of the moving cell overlapped with the final cell *A*, Eq. (7), is based on the energy $v|_{j+1}$, and that with the final cell *B*, Eq. (8), is based on $v|_j$. Similarly, the percentages according to Eq. (9) and Eq. (10) can be obtained for the scattered particles within final cells *C* and *D*. Usually, after the collision, the fraction of scattered particles for the part of the moving cell overlapped with the spatial cell $z|_i$ will be different from that for the part of the moving cell overlapped with the spatial cell $z|_{i+1}$, because the scattering rates were different in the different spatial cells.

For the CS with LLMC's, when the moving cell moves to a new position after the next time step, the particle density in the moving cell will be assumed uniform over space. The inconsistency can be removed if the kinetic energy (or the velocity $v'$) based on the CFP at position $z'$ is used to determine the number of scattered particles. After this CFP adjustment, the particle density will always be uniform within a moving cell since the density of the scattered particles is removed uniformly within a moving cell. For the regular CS implementation, the CFP adjustment is not necessary. If moving cells are used, the result with the CFP adjustment will be much smoother than the result without it, where bumps and spikes in the density profile are observed. However, energy conservation can be violated when scattered particles are put back to the mesh cells whose potentials are different from the potential at the center of the LLMC, if their kinetic energy is that found based on the CFP at $z'$ (the center of the moving cell). Especially in high-pressure cases, high collision rates exacerbate the violation of conservation of energy, which occurs with the CFP used in this way. Using the CFP in this way, the regular CS frequently does not give a convergent result, so the staircase potential must be employed. The LLMC method seems to be unaffected by use of the CFP for finding the kinetic energy of scattered particles but the use of the staircase to find the energy for replacement on the mesh may be more accurate. The staircase potential is always used when replacing unscattered particles on the mesh.

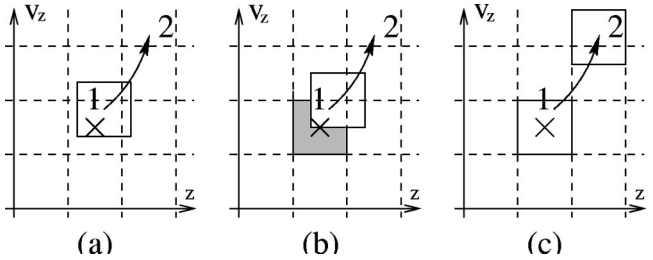


FIG. 5. Procedure for launching a new moving cell.

In addition to the above, we now describe other possibilities to implement the CS with LLMC's. To avoid launching a moving cell for each mesh cell at each time step, in one version a new moving cell is launched only if the moving cell deviates from the original mesh cell too much. As shown in Fig. 5, the moving cell in position 1 can still represent the mesh cell (marked $\times$), so distributed particles from other moving cells are placed in this moving cell instead of (or after being put in) the mesh cell. When the moving cell deviates from the mesh cell such that the ''center'' of the moving cell is not in the range of the mesh cell, a new ''moving cell'' is launched as shown in Fig. 5(b). Since this new cell is meant to represent the mesh cell at the moment, it is held fixed in phase space at first, and distributed particles from other moving cells go into this new cell instead of the almost-left moving cell. In Fig. 5(c), as the moving cell reaches position 2, it has totally left the range of the mesh cell marked $\times$, so the newly launched moving cell begins to join the motion. In Fig. 5 the criteria for the transitions from phase (a) to phase (b) and from phase (b) to phase (c) depend on how cells are moved in the ballistic motion.

### C. Cell faces or cell centers

Two cases have been considered: the spatial cell boundaries/faces at $z|_j-\Delta z|_j/2$ and $z|_j+\Delta z|_j/2$ can be moved either (i) together according to the initial velocity and local electric field at the cell center or (ii) independently according to the initial velocity and local electric field at each face position. In the first case (the two spatial faces of a cell are moved together), if a cell with initial coordinates $(z,v,\mu)$ moves to $(z',v',\mu')$, the final spatial position is obtained from Newton's law:

$$z'=z+(v\mu)\Delta t+\frac{q}{2m}E(z)(\Delta t)^2,$$

and the conservation of the ''$z$-component of energy'' $\epsilon_z$ gives:

$$\epsilon_z=q\Phi(z)+\frac{m}{2}v_z^2=q\Phi(z')+\frac{m}{2}(v_z')^2, \tag{11}$$

where $v_z = v \times \mu$, $v_z' = v' \times \mu'$, and $v[1-(\mu)^2]^{1/2} = v'[1-(\mu')^2]^{1/2}$ is the perpendicular velocity. Similarly, if $z|_j'$ is energetically forbidden, the particles retrace their trajectory to the previous spatial cell (i.e., the cell next to the cell where the particles first are forbidden to be), reversing the sign of $v_z$. Since the potential, $\Phi(z|_j)$, is constant in space in the spatial cell $j$, $\Phi(z)$ and $\Phi(z')$ correspond to $\Phi(z|_j)$ and $\Phi(z|_j')$, respectively. There are spatial gaps between the moving cells originating from the same mesh cell, if the two spatial faces of a cell move based on the information at the cell center. However, this phenomenon cannot easily be eliminated even when the two spatial faces are moved independently. The criterion for the phase (a)-to-phase (b) transition is intended to check if the faces of the moving cell pass the *center* of the mesh cell in space. The criterion for the phase (b)-to-phase (c) transition is to check if the faces of the moving cell *totally* leave the mesh cell in space. Phase (a)-to-phase (b) and phase (b)-to-phase (c) transitions may occur at the same time since cells are treated as discrete values in velocity.

In the second case (the two spatial faces of a cell are moved independently), the two spatial faces can have totally different behavior. Before a time step of the ballistic motion, if an initial cell is launched at the mesh cell $(j,l,k)$, the two faces of this initial cell have the same perpendicular velocity $v|_l\sqrt{1-\mu|_k^2}$ and the same $z$-component of velocity $v|_l\mu|_k$; however, later on the two faces of an initial cell will ''keep track'' of their own velocities, i.e., a moving cell might have different velocities for its two faces. Similar to the first case, the velocity of each face of a moving cell after a time step is determined by conserving the ''$z$-component of energy $\epsilon_z$'' as in equation (11). In other words, each spatial face has its own position in the three-dimensional space $(z,v,\mu)$. Since cell faces are moving independently and the electrostatic potential is (often) step-function like, there might exist gaps between moving cells. For example, the back face of one cell is the front face of another cell initially, but they move according to the potential associated with different cells. At the end of the time step, the front face of the cell and the back face of the next cell will have different velocities. Gaps will develop at the end of the next time step. This is one of the finite mesh size effects. Sometimes a moving cell may occupy many final spatial cells; $\epsilon_z$ is assumed to vary linearly between two faces (since we do not calculate $\epsilon_z$ except at the faces). The same assumption also allows us to find the perpendicular component of velocity. The different parts of the moving cell in different final spatial cells have their $v$ and $\mu$ determined by the linearly interpolated perpendicular component of the velocity $v[1-\mu^2]^{1/2}$ and the $z$-component of velocity $v\mu$, which is calculated from the linearly varying $\epsilon_z$. The motion of faces of the moving cell gives the same criterion for phase (a)-to-phase (b) and phase (b)-to-phase (c) transitions. If one of the faces has its velocity pointing one way out of the mesh cell but the other face has its velocity the other way, then we invoke the phase (a)-to-phase (b) transition. If both faces have their velocities out of the mesh cell in the same direction, then we invoke the phase (b)-to-phase (c) transition.

Had we allowed particles to be uniformly distributed over $v$ and $\mu$, remapping after the ballistic motion using this uniformity to do the mapping would destroy this ''uniformity'' assumption (or else it would lead to nonconservation of energy, etc., if we enforced uniformity) unless more variables are used to record this nonuniformity for each cell. But as one can see in the simple one-dimensional water-bag model by Berk *et al.* [15], the number of required recording variables will soon exceed the computer memory limit. Hence, we treat a cell as a single point in velocity but with a finite extent in space.

### D. Ion ballistic motion

The ''ballistic'' move for ions is similar to that described above, however, the final velocity for the ions is found using the equation of motion without total energy conservation, since conservation of momentum is more important for ion dynamics. The (ion) particles of a moved cell are instead put back to the overlapped mesh cells according to the conservation of momentum. The ion distribution function has only two phase-space dimensions, namely, $(z,v_z)$. The components of the velocities of the ions which are not explicitly tracked are assumed to have a Maxwellian distribution at the background gas temperature.

### E. Collisions and gas phase processes

Helium plasma illustrates the typical processes taking place in a discharge. The collision part of the propagator in the CS is straightforward once the collision operator is constructed [6]. Since particles are placed on mesh cells after ballistic motion and collisions, a pre-computed collision operator for discrete values of $v$ and $\mu$ can be very efficient.

Elastic collisions of electrons with neutral atoms are typically anisotropic in nature. Two versions of the elastic collision operator are used. The ''full'' version provides an anisotropic distribution with recoil cooling also. In the center of mass ($C$) frame the differential cross section only depends on the initial relative velocity of the electron with the reduced mass, $mM_g/(m+M_g)$, and the scattering angle $\Theta$, where $m$ is the electron mass and $M_g$ is the background neutral mass. The azimuthal scattering angle is uniformly distributed, so we are only concerned with the polar angle to which the electron scattered. For incident electrons with initial velocity $v$ into the background neutrals with temperature $T_g$ in the lab ($L$) frame, the average relative kinetic energy in the $C$ frame is given by

$$\tau_0 = \frac{1}{2}\frac{mM_g}{m+M_g}\left(v^2 + \frac{3k_BT_g}{M_g}\right), \tag{12}$$

where $k_B$ is the Boltzmann constant and $T_g$ is the background gas temperature. The fraction of electrons elastically scattered out of a cell with coordinates $(z,v,\mu)$ during a time step $\Delta t$ is

$$\frac{n_{sc}}{n_{cell}} = \Delta t N_g \langle \sigma(\tau_{rel}) v_{rel} \rangle \tag{13}$$

$$\approx \Delta t N_g \langle \sigma(\tau_0) \rangle \sqrt{v^2 + 3k_BT_g/M_g}, \tag{14}$$

where $N_g$ is the number density of the background gas and $\langle \cdot \rangle$ averages over the background Maxwellian neutrals.

Since the elastic collision is kinetic energy conservative, the transformation between the scattering angle $\theta$ in the $L$ frame and the angle $\Theta$ in the $C$ frame is given by

$$\tan\theta = \frac{\sin\Theta}{(m/M_g)+\cos\Theta}. \tag{15}$$

The final kinetic energy of the scattered electrons in the $L$ frame is given by

$$\frac{m}{2}v'^2 = \frac{m}{2}v^2\left(1-\frac{2mM_g}{(m+M_g)^2}(1-\cos\Theta)\right). \tag{16}$$

For electron collisions with neutrals, $m \ll M_g$ and we obtain $\theta \approx \Theta$. If the differential scattering cross section is constant with respect to the angle $\Theta$, we can construct the average cosine of the scattering angle $\theta$ from

$$\langle\mu(\tau_0)\rangle = \frac{1}{\sigma(\tau_0)}\int_{-1}^{1}\mu'\frac{d\sigma(\tau_0)}{d\mu'}d\mu', \tag{17}$$

where $d\sigma(\tau_0)/d\mu'$ is the differential cross section, and the total cross section is given by

$$\sigma(\tau_0) = \int_{-1}^{1}\frac{d\sigma(\tau_0)}{d\mu'}d\mu'. \tag{18}$$

Averaged over $\theta$ the kinetic energy of the scattered electrons is proportional to:

$$v'^2 = v^2\left(1-\frac{2m}{M_g}[1-\langle\mu'(\tau_0)\rangle]\right). \tag{19}$$

This ''simplified'' version provides isotropic distribution of scattered electrons with energy transfer due to recoil during electron-atom collisions. We note that the definition of the momentum transfer cross section can be expressed in terms of $\langle\mu'(\tau_0)\rangle$ as

$$\sigma_{MT}(\tau_0) = \int_{-1}^{1}(1-\mu')\frac{d\sigma(\tau_0)}{d\mu'}d\mu' = \sigma(\tau_0)[1-\langle\mu'(\tau_0)\rangle]. \tag{20}$$

We emphasize that we will use $\sigma(\tau_0)$ to determine the collision rate, and in most cases $\sigma(\tau_0) > \sigma_{MT}(\tau_0)$. The speed of the electron will on average change, due to elastic recoil cooling, to a value given by

$$v' = \left[v^2-[1-\langle\mu'(\tau_0)\rangle]\frac{4}{M}\left(\frac{1}{2}mv^2-\frac{3}{2}k_BT_g\right)\right]^{1/2}. \tag{21}$$

Unlike elastic electron-neutral atom collisions, differential cross sections are rarely available for inelastic electron-neutral atom collisions. We introduce a parameter $h$, which is the fraction of the average $z$ momentum of the electron that is conserved in inelastic collisions. The average final velocity component along the incident direction for this set of electrons can be cast into the form

$$v_f = \mu_0 h\left(v_0^2-\frac{2\tau_g}{m}\right)^{1/2}, \tag{22}$$

where $\tau_g$ is the energy given up in the collision. Because the lack of the information as to differential cross-section data, the parameter $h$ would, based on simple physical arguments, vary from near zero at threshold energies to near unity at high energies. For the ''simplified'' version, an isotropic treatment is employed.

Once the electron velocity is less than the characteristic atomic velocity $Ze^2/4\pi\epsilon_0$, which corresponds to about 27.3 eV, the polarization scattering affects the elastic collisions between electrons and neutrals with the potential [16]

$$U(r) = -\frac{q^2a^3}{8\pi\epsilon_0 r^4}. \tag{23}$$

For electrons with higher energy, hard sphere collisions apply. Similarly, the Coulomb scattering between charged particles is described by the well-known formulas:

$$\frac{d\boldsymbol{v}_\alpha}{dt} = -(1+m_\alpha/m_\beta)\psi(x^{\alpha\backslash\beta})\nu_0^{\alpha\backslash\beta}\boldsymbol{v}_\alpha \tag{24}$$

$$\frac{d(\boldsymbol{v}_\alpha-\langle\boldsymbol{v}_\alpha\rangle)_\perp^2}{dt} = 2[(1-1/2x^{\alpha\backslash\beta})\psi(x^{\alpha\backslash\beta}) + \psi'(x^{\alpha\backslash\beta})]\nu_0^{\alpha\backslash\beta}v_\alpha^2 \tag{25}$$

$$\frac{d(\boldsymbol{v}_\alpha-\langle\boldsymbol{v}_\alpha\rangle)_\parallel^2}{dt} = [\psi(x^{\alpha\backslash\beta})/x^{\alpha\backslash\beta}]\nu_0^{\alpha\backslash\beta}v_\alpha^2 \tag{26}$$

$$\frac{dv_\alpha^2}{dt} = 2[(m_\alpha/m_\beta)\psi(x^{\alpha\backslash\beta})-\psi'(x^{\alpha\backslash\beta})]\nu_0^{\alpha\backslash\beta}v_\alpha^2, \tag{27}$$

where

$$\nu_0^{\alpha\backslash\beta} = \frac{4\pi q_\alpha^2 q_\beta^2 n_\beta \ln\Lambda_{\alpha\beta}}{(4\pi\epsilon_0)^2 m_\alpha^2 v_\alpha^3} \tag{28}$$

$$x^{\alpha\backslash\beta} = m_\beta v_\alpha^2/2k_BT_\beta \tag{29}$$

$$\psi(x) = \frac{2}{\sqrt{\pi}}\int_0^x dt\, t^{1/2}e^{-t} \tag{30}$$

$$\psi'(x) = \frac{d\psi}{dx}, \tag{31}$$

and $\ln\Lambda_{\alpha\beta}$ is the Coulomb logarithm. In general, kinetic effects of a collison process can be described by

$$\frac{d\boldsymbol{v}_\alpha}{dt} = -\nu_s^{\alpha\backslash\beta}\boldsymbol{v}_\alpha \tag{32}$$

$$\frac{d(\boldsymbol{v}_\alpha-\langle\boldsymbol{v}_\alpha\rangle)_\perp^2}{dt} = \nu_\perp^{\alpha\backslash\beta}v_\alpha^2 \tag{33}$$

$$\frac{d(\boldsymbol{v}_\alpha-\langle\boldsymbol{v}_\alpha\rangle)_\parallel^2}{dt} = \nu_\parallel^{\alpha\backslash\beta}v_\alpha^2 \tag{34}$$

$$\frac{dv_\alpha^2}{dt} = \nu_\epsilon^{\alpha\backslash\beta} v_\alpha^2, \tag{35}$$

where the collsion frequencies, $\nu_s^{\alpha\backslash\beta}$, $\nu_\perp^{\alpha\backslash\beta}$, $\nu_\parallel^{\alpha\backslash\beta}$, and $\nu_\epsilon^{\alpha\backslash\beta}$ are averaged over the distribution of the background particles $\beta$. As we can see, the theoretical diffusion in pitch angle $\mu$ is predicted by Eq. (33), and the diffusion in velocity $v$ is predicted by Eq. (34). The drag force due to the background particles is represented as Eq. (32). The elastic cooling amounts to the energy loss, Eq. (35). From Eq. (34), if the energy mesh is fine enough such that $\Delta v_\alpha^2/v_\alpha^2 = \Delta v_\alpha/v_\alpha < \nu_\parallel^{\alpha\backslash\beta}\Delta t$, then the physical diffusion will dominate the numerical diffusion. This was achieved by choosing a longer time step instead of decreasing the mesh cell size.

The total and differential cross-section data for electron-helium elastic scattering are taken from LaBahn and Callaway [17,18]. The differential elastic cross section has an estimated accuracy $\pm 5\%$. For electron-helium ionization collisions, since the second ionization is at about 70 eV where the electron population is small, only single ionization is considered [19]. The electron-helium excitation and ionization cross section data are taken from Alkhazov [20]. All inelastic scattering processes are assumed isotropic. Transitions $1^1S$–$n^1S$, $1^1S$–$n^1D$, $1^1S$–$n^3S$, $1^1S$–$n^3D$, and $1^1S$–$n^3P$, where $2 \leqslant n \leqslant 5$ and is allowed by the selection rules, are included, though transitions between excited states are ignored. The semi-empirical inelastic cross sections have an uncertainty of $\pm 25\%$ at low impact energies and $\pm 5\%$ at higher energies where the Born approximation is reliable. For rf discharges, simulations under the same pressures and driving voltages are also carried out using benchmark cross-section formulas from Ref. [21] for elastic electron-helium scattering, for electron-helium ionization scattering, and for electron-helium excitation scattering.

Total cross sections for electron transitions between excited states of helium are taken from Fon *et al.* [22]. The charge exchange cross section of $He^+$ and He is taken from Helm [23].

### F. Numerical implementation

The recipe given here will be used as a guideline for CS implementation. Analysis and justification of steps in the recipe will be given afterwards.

*Recipe:*

*(1) Find constants of motion*. These conserved quantities should remain constant for both the ballistic motion and the remapping rules. It may be impossible to satisfy all conservation laws due to the finite mesh size effects; that is, while we are conserving one quantity the discreteness of the mesh leads to a change of another. Hence, the priority of these constants of motion is important and usually is determined by the particular physical problem. For example, in a model with one dimension in space ($z$) and two dimensions in velocity ($v_z, v_\perp$), the perpendicular component of kinetic energy $v_\perp^2$ is a constant of motion.

*(2) Choose mesh coordinates*. If a mesh coordinate is a constant of the motion, the re-mapping procedures in the CS should not distribute particles across different volumes of that coordinate. In this case, the numerical diffusion either during collisions or during ballistic motion can be reduced. For example, in a cylindrical system the radial distance and the angular momentum would be better than $r$ and $\theta$, since the angular momentum is conserved but the azimuthal angle $\theta$ is not.

*(3) Choose mesh size*. The lower kinetic-energy bound of the mesh is obviously zero, but the upper kinetic-energy bound cannot be infinite in a simulation. The population of high-energy particles is low in most cases. In addition, the cross section approaches a constant value, usually zero, at high energy. For these reasons it is justified to use a finite range for the velocity mesh. However, the mesh range should be large enough to include electrons that are involved in important processes. For example, in an rf discharge with driving voltage of 100 Volts, the highest energy cell should represent particles with kinetic energy of 100 eV at least. (Particles with energy greater than the maximum are replaced with the maximum.) The mesh size should also be fine enough in the regions of interest. (Typically we choose $\Delta v/v = \text{constant}$, $\Delta\mu = \text{constant}$, and use 10 to 20 $\mu$-cells. If we use $\Delta v_z/v_z = \text{constant}$, $\Delta v_\perp/v_\perp = \text{constant}$, we have what is probably worse resolution for the same number of mesh points.) On the spatial mesh, the mesh size may need to be kept at the order of the Debye length to resolve the sheath dynamics correctly. To resolve the velocity mesh appropriately [6], such that

$$\frac{\Delta v}{v} = C, \tag{36}$$

the boundaries of the velocity cells can be obtained by simply ''integrating'' the above equation:

$$v|_l = v_{\min} \exp\{C' l\}, \quad l = 0, \ldots, n_l, \tag{37}$$

where $c'$ is chosen to make the constant $C$ about 0.1. The lowest cell is at $v = 0$; the next is usually at about room temperature such that $\frac{1}{2} m v_{\min}^2 \approx 0.026$ eV.

*(4) Remapping rules*. Particles are assumed uniformly distributed over space, within each moving cell. The various spatial parts of a moving cell can have different velocities ($v_z, v_\perp$), if they are in different spatial cells. If conservation of energy is the most important conservation law, then we can transform to an energy mesh instead of a velocity mesh when we map particles from various parts of the moving cell to their corresponding final cells with the same spatial position. (This is equivalent to the rule given above—see Fig. 4.) Since particles are remapped to the mesh cells, which are discrete, this may cause other constants of the motion to be changed.

*(5) Ballistic motion*. The equations of motion can be integrated using the Euler scheme, or others. Since conservation of energy is emphasized for electrons, the value of the velocity used to do remapping of electrons is not determined by integrating the equations of motion, but by conservation of energy. The conservation of momentum law is usually employed for ions.

*(6) Collisions*. Differential scattering cross-section data are rarely available, so inelastic scattering, like ionization and excitation, is usually assumed to be isotropic.

*(7) Time step*. For the simulation of a plasma, at least three basic characteristic frequencies restrict the time step

$\Delta t$. To avoid running out of particles, there should be at most one collision in a time step; the time step $\Delta t$ must satisfy the relation

$$\Delta t \ll \nu_s^{-1} = [N v_{rel} \sigma_{tot}(v_{rel})]^{-1}, \tag{38}$$

where $N$ is the density of scatterers, $v_{rel}$ is the relative speed, and $\sigma_{tot}(v_{rel})$ is the total cross section. The total collision time $\tau = \nu^{-1}$ can be obtained as

$$\frac{1}{\tau} = \sum_{i}^{\text{all processes}} \frac{1}{\tau_i}.$$

Usually $\Delta t \sim 0.2\tau < e^{-1}\tau < \tau$. To resolve the dynamic behavior of electrons, which are the fast species in a processing plasma, the time step should be less than plasma characteristic time scale,

$$\Delta t < \frac{2\pi}{\omega_e} = 2\pi \left( \frac{ne^2}{\epsilon_0 m} \right)^{-1/2}, \tag{39}$$

where $m$ is the electron mass, $n$ is the electron number density, and $e$ is the electron charge. Finally, if an external field is present, $\Delta t$ should be much less than the time scale of the external field: $\Delta t < 2\pi/\omega$, where $\omega$ is the angular frequency of the external field. If the electromagnetic fields vary rapidly in a time-varying system, the time step is limited by the field period. However, this restriction is imposed by the electromagnetic field solver, not by the CS.

The choice of these independent variables $(z, v, \mu)$ to describe the electron distribution function is somewhat arbitrary. Another choice for phase-space coordinates is $(z, v_z, v_\perp)$. It has some advantages in ballistic motion for constant field cases, but complicates the collision processes. Most of the difficulty in programming comes from the finite mesh size effects. The variables $(v, \mu)$ and $(v_z, v_\perp)$ give rise to different amounts of diffusion if one considers a ''ballistic'' move or a ''move'' due to a collision.

In a ''ballistic'' move in a one-dimensional system $v_\perp$ is constant, so $(v_z, v_\perp)$ are useful—since the $v_\perp$ variable need not be remapped. However, $(v_z, v_\perp)$ yields low resolution of pitch angle for low-energy cells and uneven resolution for high-energy cells. (Pitch angle resolution of $\Delta\mu \sim 0.1$ is probably adequate for all $v$.)

In a purely collisional move, where $v$ is exactly equal to a value that lies on the mesh, then if the collision does not change $v$, only $\mu$ varies so only it has to be remapped. For moving cells, if we follow the moving cell for about a collision time, $v$ is not likely to match a value on the mesh. Thus when we remap after the collision there is some diffusion in $v$ as well as $\mu$. For this reason, there is no great advantage to following the moving cell for longer than a collision time—collisions are already introducing errors. The $(v, \mu)$ pair still offer an advantage, in this case—because the phase space is more efficiently partitioned using these variables. When LLMC's are used, the collisions cause most of the numerical diffusion. It is thus helpful to use $(z, v, \mu)$, which sometimes reduces numerical diffusion in collisions. The main reason these variables reduce diffusion, however, is that the $\mu$ variable needs fewer cells than (say) $v_\perp$, freeing memory for better resolution in $v$.

### G. Merging moving cells

We have considered limiting the number of moving cells by merging nearby (in phase space) moving cells, which originate from the same initial cell, into a composite cell, using conservation laws to determine the characteristics of the new moving cell. It is essential to ensure that such a merging does not move the particles in space (i.e., the density in each spatial cell must be the same before and after the merge). This is to ensure that artificial currents are not created—including displacement currents, and spurious electric fields. This merging is in some sense very similar to simply remapping moving cells onto the fixed mesh, and then (as usual) launching moving cells from the fixed cells. As long as the fixed mesh has adequate resolution, remapping is more straightforward, since it uses the existing procedures, and so is probably preferable. The low-energy moving cells are unlikely to merge because the velocity does not stay within the fixed cell. The high-energy cells are unlikely to merge because moving cells leave the fixed cell in space. However, merging does not always seem to give a stable result. As an alternative, it was found that launching moving cells only every second time step produced no noticeable effect on the simulation; further delays in launching appear to alter the simulation.

### H. Numerical diffusion

Since the moving cells are remapped periodically, if a moving cell should stay at roughly the same velocity during its lifetime, the numerical diffusion in velocity space can be estimated by a random-walk picture of diffusion with the diffusion coefficient in velocity space:

$$D_v = \frac{1}{2} \left( \frac{\Delta v}{2} \right)^2 \nu_{\text{rep}}, \tag{40}$$

where $\nu_{\text{rep}}$ (set to $v/\delta x$ or $\nu_{\text{el}}$) is the replacement frequency of mapping back moving cells in the CS. From the velocity resolution Eq. (36), if the parallel ($z$) component of the velocity is in reality nearly constant, then the above equation can be expressed as:

$$D_v = \frac{1}{8} \frac{C^2 v^3 \mu}{\delta x}, \tag{41}$$

where $\delta x$ is the distance traveled by the moving cell before mapping back.

The diffusion in velocity space for particles moving across the system can be cast as:

$$\delta v = \sqrt{2 D_v t_{\text{diff}}}, \tag{42}$$

and

$$t_{\text{diff}} = N \tau_{\text{coll}} = \frac{L^2}{\lambda^2} \tau_{\text{coll}} = \frac{L^2}{v^2} \nu_{\text{coll}},$$

where $N=L^2/\lambda^2$ is the number of collisions before the particles diffuse across the system, $L$ is the system dimension, and $\lambda$ is the elastic scattering mean-free path. So the numerical diffusion in $v$, before particles cross the system, will change $v$ by

$$\delta v = \frac{L\Delta v}{2v}\sqrt{\nu_{\rm rep}\nu_{\rm coll}}, \tag{43}$$

where $\nu_{\rm rep}=v/\delta x$ or $\nu_{\rm el}$ (see below) and $\nu_{\rm coll}=1/\tau_{\rm coll}$ is the elastic-scattering frequency. This expression for $\delta v$ was used to check that numerical diffusion gave a smaller change in $v$ than the dominant physical processes, in the simulations that follow.

#### I. Number of moving cells

The number of moving cells on the train for an initial cell is chosen as the minimal of the number of the time steps in a collision time, and the number of the time steps for the cell to travel one spatial cell based on the initial velocity. However, to reduce moving cells to a reasonable number for those initial cells with low $\mu$ value, an upper limit is also imposed: usually, 30 moving cells will highly reduce the numerical diffusion and give good simulation results. More moving cells can be used depending on the computer memory resource and on computation time.

### III. SIMULATION RESULTS AND DISCUSSION

We will present two sets of benchmark tests, for the CS with LLMC's: a ''swarm'' experiment, which is a discharge with a spatially uniform electric field, and rf capacitive discharge simulations. We shall see that the use of LLMC's produces an improvment in accuracy, in less collisional cases.

Helium gas is used in these benchmark tests, since the physical and chemical processes involved are relatively simple so that we can concentrate on the effects of the CS with LLMC's.

#### A. Swarm simulation

A typical swarm experiment is a one-dimensional axially symmetric system. The electrons are accelerated by the applied electric field in a weakly ionized gas. We shall simulate swarm experiments, using the CS with LLMC's, for the parameter $E/N$ in the range from 8 to 282 Td (where 1 Td $=10^{-17}$ V cm$^2$) at room temperature, 293.15 K. Since ion dynamics are not important in these swarm simulations, they are ignored and the secondary electrons are assumed to be emitted from the cathode monoenergetically. Rigorously, the secondary electron energy should be spread in a certain range. To speed up the convergence, a constant number of electrons are assumed to be ejected from the cathode with energy equal to that of the lowest energy cell, and along the positive $z$-direction ($\mu=1$). The differential cross section for anisotropic elastic scattering is integrated over the scattering angle, as Eq. (20) to give an isotropic momentum transfer cross section. Elastic scatterings are treated as being isotropic but using the momentum transfer cross section to yield the correct drift velocity for electrons. For simplicity,

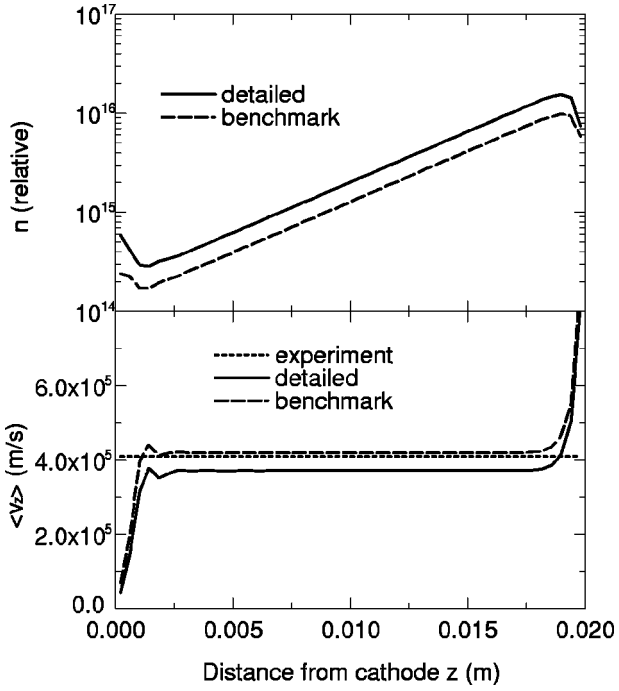


FIG. 6. Electron density and average velocity: The solid line denotes the result using detailed cross-section data, the thicker dashed line indicates the result using benchmark cross-section data. The other dashed line is read from experimental data. $E/N=200$ Td.

excitation processes have been separated into two groups. The transition from the ground state to the $2^3S$ state has the threshold energy 19.82 eV. The loss of electron energy for other excitation processes is averaged over all the above transitions and set up with the threshold energy 21.5 eV. In the benchmark cross-section data, all excitation processes are simplified to one representative process with threshold 19.8 eV [21]. The convergence criterion is set such that the electron density fraction changes less than $10^{-3}$ in one time step. The separation of the two parallel plates is 2 cm, and the dc voltage drop between them is 400 Volts for all simulations. Changing the background gas pressure will give the desired range of $E/N$. However we note that exact voltages and gas pressures in the experiments are not always available. Using different pressures, while keeping the same $E/N$ ratio, may result in different swarm parameters.

The simulation result for the $E/N=200$ Td case is shown in Fig. 6 to Fig. 7. Results from swarm experiments compiled by Kücükarpaci *et al.* [24] are also displayed. Care has been taken to ensure a proper comparison of the flow velocity $\langle v_z\rangle$ from the CS with the experimentally-obtained drift velocity $v_d$ (often denoted as $W$). Even though there is some debate about the velocities measured in experiments, the two velocities are related by the following equation:

$$\langle v_z\rangle = v_d - D_L\alpha, \tag{44}$$

where $D_L$ is the longitudinal diffusion coefficient, $\alpha$ is *the first Townsend ionization coefficient*, and the operator $\langle\cdot\rangle$ averages over the velocity distribution. We take the mean value of the average kinetic energies before collisions and after collisions. Then the value, $D_L/\mu$, can be easily constructed from the Einstein relation:

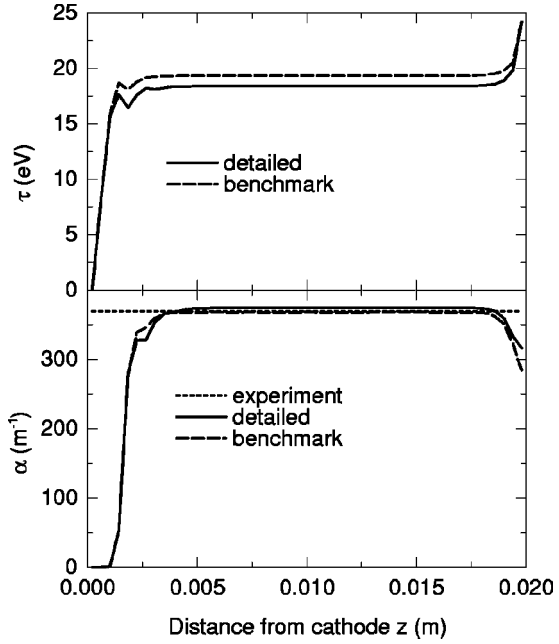


FIG. 7. Average kinetic energy and ionization coefficient: The solid line denotes the result using detailed cross-section data, the thicker dashed line indicates the result using benchmark cross-section data. The other dashed line is read from experimental data. $E/N=200$ Td.

$$\frac{D_L}{\mu}=\frac{k_B T_e/m\nu_m}{q/m\nu_m}=\frac{\langle mv^2\rangle}{3q}, \tag{45}$$

where $\nu_m$ is the momentum transfer collision rate and $m$ and $q$ are the electron mass and charge, respectively. Originally, the ionization coefficient $\alpha$ is defined through the relation: $I=I_0\exp\{\alpha(d-d_0)\}$, where $I$ is the current at the distance $d$ from the cathode, and $d_0$ is the effective distance, which accounts for the fact that electrons emitted from the cathode attain a steady state, determined by the value of $E/N$ in the gas, only after a number of collisions. Alternatively, $\alpha/N_g$ can be approximated [25], if diffusion is neglected, as:

$$\frac{\alpha}{N_g}=\frac{\langle\sigma_i(v)v\rangle}{\langle v_z\rangle}, \tag{46}$$

where $N_g$ is the helium atom number density, and $\sigma_i$ is the ionization cross section.

As shown in Fig. 6, the density of electrons grows exponentially with distance from the cathode. The results using the benchmark momentum transfer cross section for electron-helium elastic scattering are somewhat lower than the detailed momentum transfer cross section. The ionization coefficients from both simulations are essentially the same (see Fig. 7). The drift velocity $v_d$ is higher in the case where the benchmark cross-section data are used. The same effect is also reflected in the average kinetic energy (see Fig. 7). The measured data agree better with the simulations at higher pressures, where it is a good approximation that swarm parameters are functions of $E/N$. The first Townsend coefficient expressed as a function of $E/N$ is shown in Fig. 8. In the low $E/N$ range, where the pressure is high, the premise of low diffusion, made to obtain Eq. (46), is no longer satisfied. If we interpret the slope the density profile plot as $\alpha$, then we get a considerably better fit to the experimental data. (Recently, a set of swarm parameters, such as drift velocity and ionization coefficient were obtained with a new technique using photoelectrons induced by a pulse laser [26]. Under different helium gas pressures, the electron drift velocity may show an order of 3 difference in some ranges of $E/N$.)

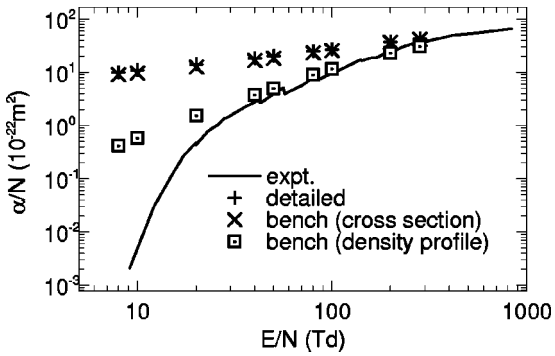


FIG. 8. The ratio of the first Townsend coefficient to the neutral density: Detailed cross-section data are used in these swarm experiments. The first Townsend coefficient is also obtained by two different methods of $\alpha/N$ calculation, using benchmark cross-section data. The solid line is read from experimental data.

From these simulation results, the CS with LLMC's appears to agree with experimental data well. However, errors in scattering cross section data and the effect of pressure difference between simulations and experiments may cause the deviation of simulation results from the experimentally-measured values. The regular CS shows similar simulation results—with differences being of the order of 5%. Since swarm experiments are performed under high pressures, high collision rates suppress the advantage of the CS with LLMC's over the regular CS. The regular CS is more efficient for simulating discharges at high pressures.

### B. RF discharges

As pointed out by Levitskii [27], at low rf discharge voltages ionization is provided by plasma electrons, which is called the $\alpha$ mode, while at high discharge voltages ionization is maintained by fast electrons initiated at the rf electrodes (including the secondary electrons), which is called the $\gamma$ mode. In what follows, we study discharges in the $\alpha$ mode, since this calls for an accurate simulation of the heating of electrons from low energies until they reach the ionization threshold, which is a stringent test of the simulation technique. (In the $\gamma$ mode, the electrons that do the ionization are energetic as soon as, or very soon after, they enter the discharge.) In all the one-dimensional simulations of rf helium discharges here, when choosing the number of moving cells on each train we base this on the number of time steps in a collision time. For simulations in higher dimensions, the number of LLMC's on each train is limited by computer resources.

While the kinetic model we shall use for electrons is the same as in the previous section, the ions are also treated kinetically by using a two-dimensional CS. The variables $z$ and $v_z$ are used to design the mesh for ions. A room tem-

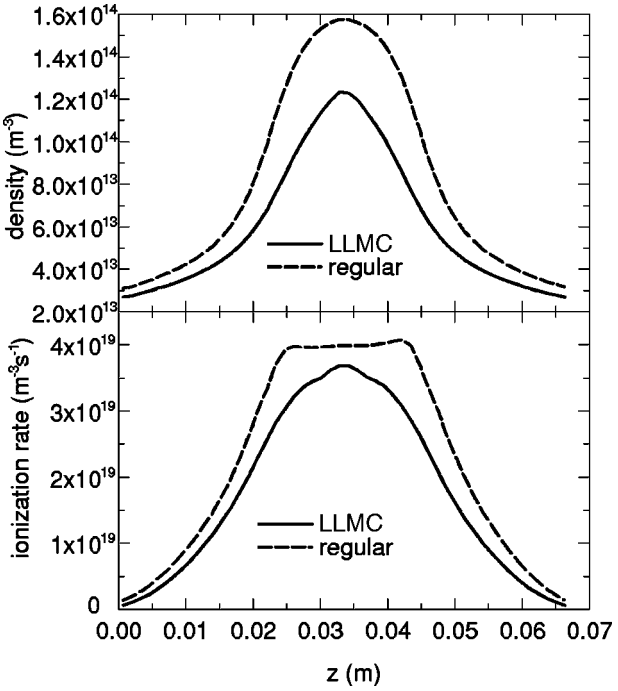


FIG. 9. Instantaneous ion density profiles and time-averaged ionization rate: Rf helium discharge at phase 0 after 120 rf cycles, $p=30$ mTorr, $V_{\rm rf}=220$ V.

perature Maxwellian distribution is assumed in the perpendicular direction for ions. The regular CS is used for ions and the $z$-component of velocity is determined from Newton's second law instead of conservation of energy. This procedure for finding velocity will guarantee the conservation of momentum. The momentum transfer cross-section data are used in the elastic collision process for ions and neutrals. Besides elastic scattering, the dominant scattering for high-energy ions is charge exchange scattering. In the CS simulations, charge exchange cross-section data are increased proportionally for low-energy ions to compensate for the elastic ion-neutral scattering (which is omitted).

Helium has two metastable levels ($2^1S$ and $2^3S$ levels) which can lead to multistep ionization. However, since the property of the CS with LLMC's is the focus of investigation, these metastable species are not tracked at the current stage.

All rf discharge benchmark simulations are carried out for the system of two parallel plates 6.7 cm apart. Three different pressures are tested with various driving voltages: 30 mTorr, 100 mTorr, and 300 mTorr. The experimental measured values are listed in Table IV of Ref. [28]. The relevant parameters are, rf voltage amplitude $V_{rf}$, plasma density in the center of the discharge $n_0$, and average electron energy in the center of the discharge $\frac{3}{2}k_bT_e^{\rm eff}$. While experimental measurements are carried out under constant rf current, simulations are usually based on constant driving voltage $V_{rf}$.

At 30 mTorr (with driving voltage 220 Volts), the rf discharge is less collisional, and the numerical diffusion might significantly affect the simulation since it might change particle velocities as fast as collisions do. The ion density profile and the time-averaged ionization rates for the regular CS and the CS with LLMC's are shown in Fig. 9.

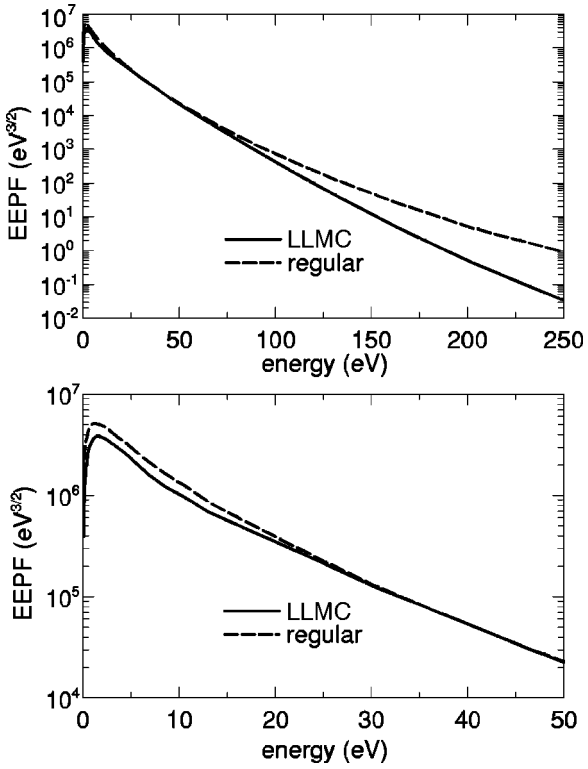


FIG. 10. Time-averaged electron energy probability function at the center of the system and the blow-up for the energy range from 0 eV to 50 eV: Rf helium discharge at phase 0 after 120 rf cycles, $p=30$ mTorr, $V_{\rm rf}=220$ V.

Usually, if the particle distribution function $f(\boldsymbol{v})$ is expressed in terms of energy $\varepsilon$ as $f(\varepsilon)$, then the *electron energy distribution function* is defined as:

$$g(\varepsilon)=f(\varepsilon)\sqrt{2\varepsilon} \tag{47}$$

$$=4\pi n\{2\pi k_BT\}^{-3/2}\exp(-\varepsilon/k_BT)\times\sqrt{2\varepsilon}\ \text{ if Maxwellian,} \tag{48}$$

where $n$ and $T$ are the particle number density and temperature, respectively. To examine the difference of the electron distribution function from the Maxwellian distribution, the *electron energy probability function* (EEPF) is defined as $g_p(\varepsilon)=\varepsilon^{-1/2}g(\varepsilon)$ and is plotted on a log scale. Thus, the

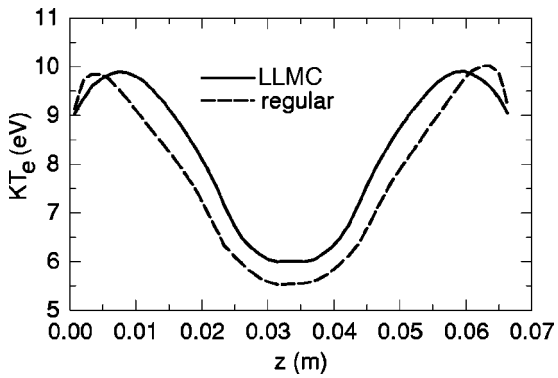


FIG. 11. Time-averaged electron ''temperature'' profile: Rf helium discharge at phase 0 after 120 rf cycles, $p=30$ mTorr, $V_{\rm rf}=220$ V.

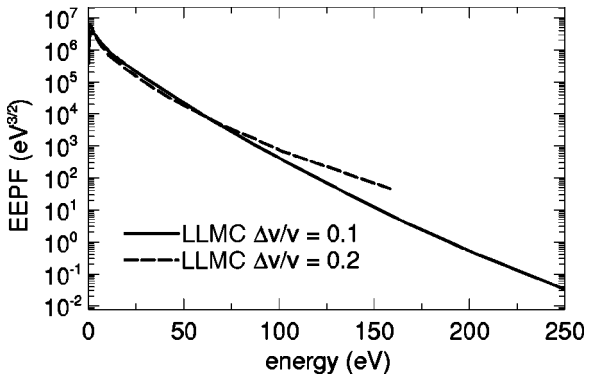


FIG. 12. Time-averaged electron energy probability function at the center of the system: Rf helium discharge at phase 0 after 120 rf cycles, $p=30$ mTorr, $V_{\mathrm{rf}}=220$ V.

occurrence of different ''temperatures'' can be observed from the slope of the EEPF log plot. The time-averaged EEPF's are shown in Fig. 10. From the EEPF plot, the regular CS shows a larger curvature, which presumably means particles tend to move to the boundaries of the energy mesh by numerical diffusion. Since inelastic collisions and recoil cooling of elastic collisions will bring electrons to the low-energy cells (Fig. 10), the CS with LLMC's will help the electrons accelerated by the electric field leave the initial mesh cell, while the regular CS frequently remaps low-energy electrons back to the zero energy cell. This can be confirmed by the time-average temperature profile (Fig. 11). Since this remapping causes more low-energy particles to pile up in the system, this partially explains why the regular CS has a higher density. The velocity (energy) mesh used in the above simulations has $\Delta v/v=0.1$. As shown in Fig. 12, with a coarser velocity mesh, where $\Delta v/v=0.2$, numerical diffusion can affect the simulation result, even though LLMC's are used.

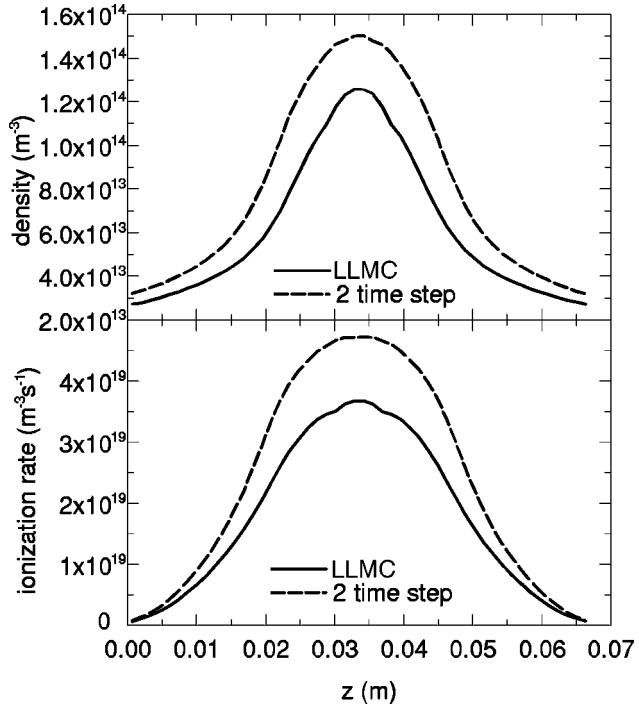


FIG. 13. Time-averaged density profile and ionization rate for two schemes: LLMC and LLMC with launching every second time step, at phase 0 after 80 rf cycles, $p=30$ mTorr, $V_{\mathrm{rf}}=220$ V.

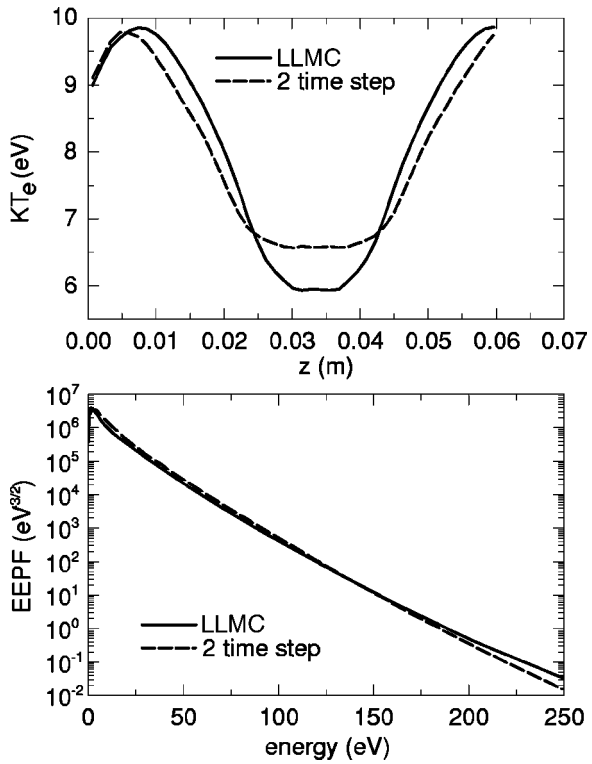


FIG. 14. Time-averaged temperature profile and EEPF for two schemes: LLMC and LLMC with launching every second time step, at phase 0 after 80 rf cycles, $p=30$ mTorr, $V_{\mathrm{rf}}=220$ V.

The ranges of the energy mesh for particle species have to be at least 220 eV. Changes of any particle species' dynam-

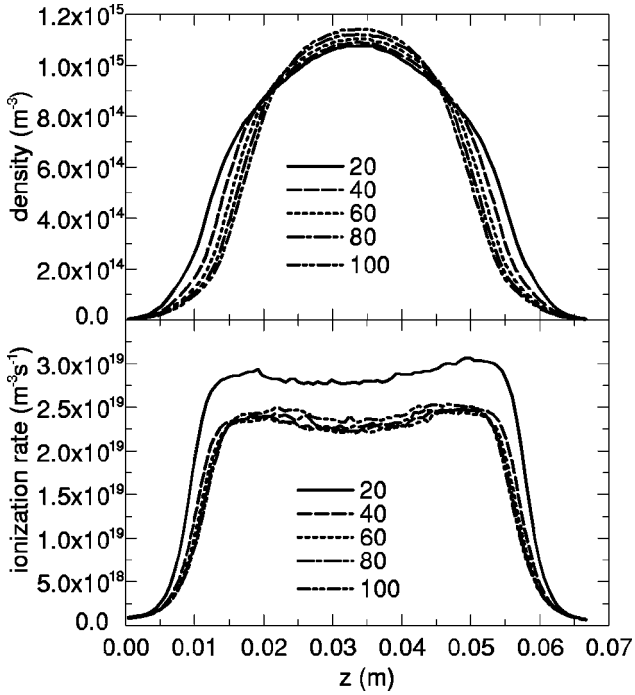


FIG. 15. Time-averaged density profile and ionization rate at various times (rf cycles): $p=100$ mTorr, $V_{\mathrm{rf}}=140$ V.

TABLE I. Plasma parameters (13.56 MHz, $L=6.7$ cm).

| $p$ (mTorr) | $V_{rf}$ (V) | $n_0$ ($m^{-3}$) | $\frac{3}{2}k_bT_e^{\text{eff}}$ (eV) | $I_{rf}$ ($Am^{-2}$) |
|---|---|---|---|---|
| 30 | 220 | $2.8\times10^{14}$ | 9.6 | 10.0 |
| 100 | 140 | $1.2\times10^{15}$ | 6.2 | 10.0 |
| 300 | 85 | $2.3\times10^{15}$ | 4.5 | 10.0 |

ics will affect the discharge dramatically. If the range of energy mesh for ions is limited to too small a value, ions may stay in the system too long and cause the density to grow incorrectly. It was necessary to expand the ion energy mesh to 220 eV (the same as the electron energy mesh), to obtain these simulation results.

If LLMC's are launched every two time steps, the results shown from Fig. 13 to Fig. 14 are obtained. Comparing the EEPF from both cases (see Fig. 14), launching every two time steps will halve the replacement frequency of LLMCs, if we use the same number of moving cells in a train, so that the numerical diffusion is highly reduced.

At 100 mTorr, the discharge is more collisional than cases at 30 mTorr. (See Table I). Since the plasma density is higher, the spatial mesh cell size has to be reduced to the order of Debye length to keep the simulation stable. Due to the higher pressure, the ionization collision frequency is higher, such that a lower driving voltage can be used to sustain the discharge. We use 140 V for the driving voltage. The evolution of various physical quantities is shown in Fig. 15 to Fig. 16. The effect of the threshold energy of various scattering processes can easily be seen from the EEPF plot. For helium gas, the single ionization threshold and various

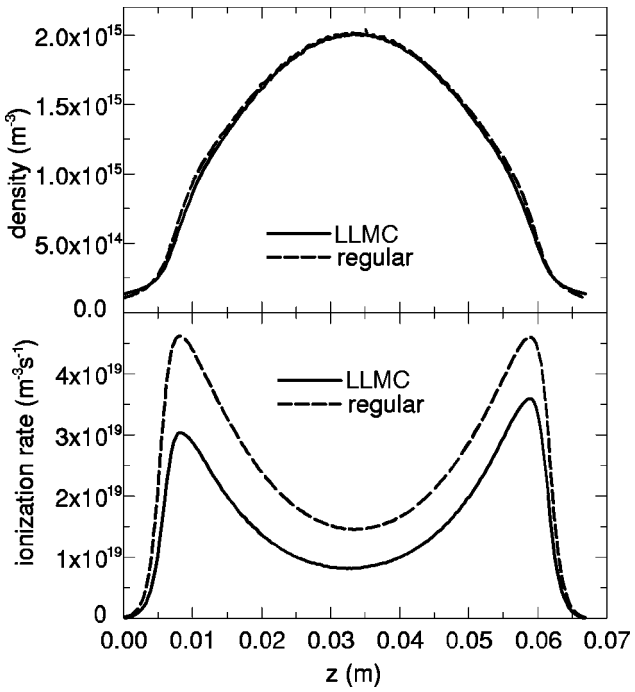


FIG. 17. Time-average ion density profile and ionization rate after 20 rf cycles: $p=300$ mTorr, $V_{\text{rf}}=85$ V.

excitation (from ground state) thresholds are about 20 eV, so electrons are depleted right after that region in the distribution function. As a result, electrons above those thresholds exhibit different ''temperatures.'' This is also seen in the data from experimental measurements [29].

At 300 mTorr the regular CS does not converge, if the CFP is used to determine the final kinetic energy of scattered

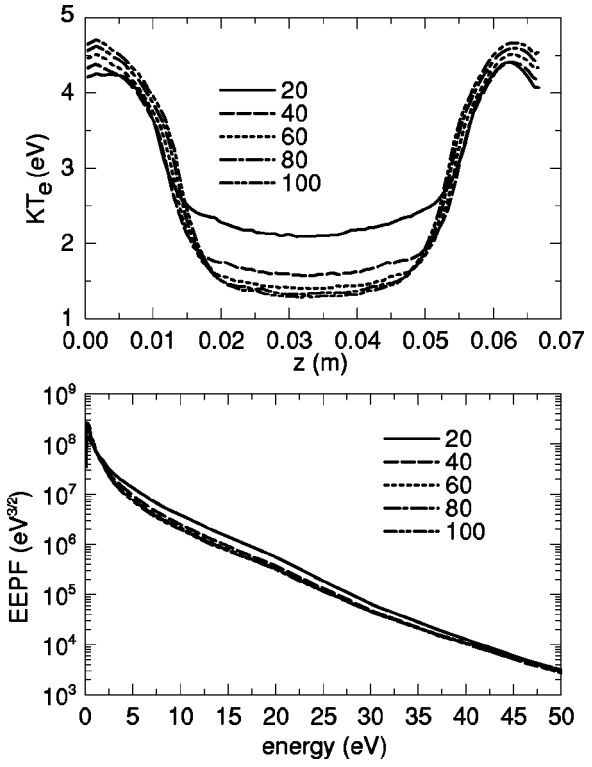


FIG. 16. Time-average temperature profile and EEPF at various times (rf cycles): $p=100$ mTorr, $V_{\text{rf}}=140$ V.

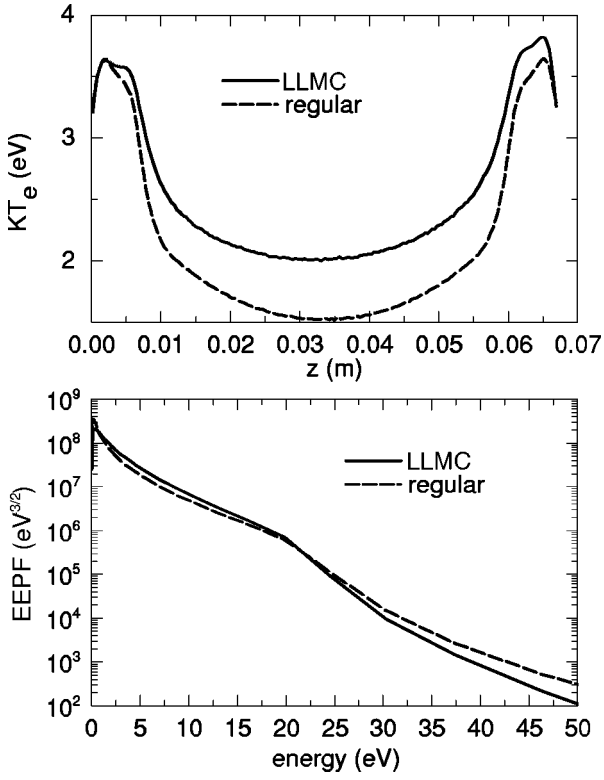


FIG. 18. Time-average temperature profile and EEPF after 20 rf cycles: $p=300$ mTorr, $V_{\text{rf}}=85$ V.

particles. Since the scattered electrons in this case are put back to the mesh cells with kinetic energy based on the CFP, violating the conservation of energy, the energy nonconservation of these scattered electrons will dominate the discharge behavior at high pressures and high scattering rates. Using the staircase potential, energy is conserved, and the regular CS gives a convergent result. As shown in Fig. 17 to Fig. 18, the regular CS and the CS with LLMC's give similar results.

### C. Discussion

The contrast between the ''regular'' CS and the CS with LLMC's can be drawn from these benchmarks. The regular CS with a staircase potential profile converges in all cases. The CS with LLMC's with a curve-fitted potential profile (for use in handling collisions, only) has advantages in reducing the numerical diffusion. In most cases, they give comparable results, the difference in every respect (density, temperature, electrostatic potential) being about 10% in steady state for rf simulations. Especially at lower pressure, it is argued that launching LLMC every second time step (or even less frequently) is appropriate. For swarm experiments and rf helium discharges at 100 mTorr or above, the high neutral gas pressure makes the discharge highly collisional. The physical diffusion will dominate numerical diffusion, so that the CS with LLMC and the regular CS will give similar results in those situations. The LLMC method can reduce the numerical diffusion on both the spatial mesh and the energy (velocity) mesh. In fact, this is crucial at low pressure to get the correct particle distribution functions, the particle temperature profiles, and many other scattering rates and chemical reaction rates. The CS with LLMC's is suitable for modeling long-mean-free path particles, for example in low-pressure high-density plasmas. The regular CS is very efficient, consumes fewer resources and is faster than the CS with LLMC's. However, the LLMC version reduces to the regular CS if only one moving cell is used. Both can provide self-consistent kinetic modeling without using *ad hoc* assumptions. The use of both methods, for comparison to each other, is probably optimal, to ensure the results obtained are reasonable.

## IV. CONCLUSIONS

We presented a detailed recipe to implement the CS with long-lived moving cells (LLMC's). An estimate of the numerical diffusion for moving cells with different kinetic energies was given. Numbers of LLMC's on trains are assigned accordingly to maintain the efficiency and accuracy of the simulations. From the simulation results of the two sets of benchmark tests, swarm experiments and rf discharges, it is seen that the CS with LLMC's can significantly reduce numerical diffusion. At high pressures, where the physical diffusion usually dominates the numerical diffusion, the regular CS consumes fewer computing resources and, hence, is more suitable. High density plasma sources, such as electron cyclotron resonance systems, usually run at low pressures, therefore, the CS with LLMC's has an advantage in simulations of these systems.


[1] C. K. Birdsall and A. B. Langdon, *Plasma Physics via Computer Simulation* (McGraw-Hill, New York, 1985).

[2] W. N. G. Hitchon, D. J. Koch, and W. D. D'haeseleer, Nucl. Fusion **29**, 1675 (1989).

[3] W. N. G. Hitchon and E. R. Keiter, J. Comput. Phys. **112**, 226 (1994).

[4] G. J. Parker, W. N. G. Hitchon, and E. R. Keiter, Phys. Rev. E **54**, 938 (1996).

[5] R. W. Hockney and J. W. Eastwood, *Computer Simulation Using Particles* (IOP Publishing, Bristol, UK, 1988).

[6] W. N. G. Hitchon, G. J. Parker, and J. E. Lawler, IEEE Trans. Plasma Sci. **21**, 228 (1993).

[7] T. Tajima, *Computational Plasma Physics: With Applications to Fusion and Astrophysics* (Addison-Wesley, Reading, MA, 1989).

[8] T. P. Armstrong, Phys. Fluids **10**, 1269 (1967).

[9] T. Armstrong and D. Montgomery, J. Appl. Phys. **1**, 425 (1967).

[10] J. P. Freidberg and T. P. Armstrong, Phys. Fluids **11**, 2669 (1968).

[11] J. B. Adams and W. N. G. Hitchon, J. Comput. Phys. **76**, 159 (1988).

[12] J. B. Adams, W. N. G. Hitchon, and L. M. Holzman, J. Vac. Sci. Technol. A **6**, 2029 (1988).

[13] D. J. Koch and W. N. G. Hitchon, Phys. Fluids B **1**, 2239 (1989).

[14] W. N. G. Hitchon, D. J. Koch, and J. B. Adams, J. Comput. Phys. **83**, 79 (1989).

[15] H. L. Berk and K. V. Roberts, Methods Comput. Phys. **9**, 88 (1970).

[16] M. A. Lieberman and A. J. Lichtenberg, *Principles of Plasma Discharges and Materials Processing* (Wiley-Interscience, New York, 1994).

[17] R. W. LaBahn and J. Callaway, Phys. Rev. **180**, 91 (1969).

[18] R. W. LaBahn and J. Callaway, Phys. Rev. A **2**, 366 (1970).

[19] V. P. Shevelko, *Atoms and Their Spectroscopic Properties* (Springer-Verlag, Berlin, 1997).

[20] G. D. Alkhazov, Zh. Tekh. Fiz. **40**, 97 (1970) [Sov. Phys. Tech. Phys. **15**, 66 (1970)].

[21] M. Surendra, Plasma Sources Sci. Technol. **4**, 56 (1995).

[22] W. C. Fon, K. A. Berrington, P. G. Burke, and A. E. Kingston, J. Phys. B **14**, 2921 (1981).

[23] S. H. Helm, J. Phys. B **10**, 3683 (1977).

[24] H. N. Kücükarpaci, H. T. Saelee, and J. Lucas, J. Phys. D **14**, 9 (1981).

[25] J. Dutton, J. Phys. Chem. Ref. Data **4**, 577 (1975).

[26] T. Sakurai, Y. Ito, T. Ueda, Y. Inoue, and H. Hori, Jpn. J. Appl. Phys., Part 1 **35**, 4525 (1996).

[27] S. M. Kevitskii, Zh. Tekh. Fiz. **27**, 1001 (1957) [Sov. Phys. Tech. Phys. **2**, 887 (1957)].

[28] M. Surendra, D. B. Graves, and I. J. Morey, Appl. Phys. Lett. **56**, 1022 (1990).

[29] V. A. Godyak, R. B. Piejak, and B. M. Alexandrovich, Phys. Rev. Lett. **68**, 40 (1992).